Available online at www.sciencedirect.com
SCIENCE DIRECT®
Biomaterials 24 (2003) 1001–1011
Biomaterials
www.elsevier.com/locate/biomaterials

Intracellular uptake of anionic superparamagnetic nanoparticles as a function of their surface coating

C. Wilhelm[a,b], C. Billotey[a,b], J. Roger[c], J.N. Pons[c], J.-C. Bacri[a,b], F. Gazeau[a,b,*]

[a] *Laboratoire des Milieux Désordonnés et Hétérogènes UMR7603, Université Pierre et Marie Curie, Tour 13, Case 86, 4 place Jussieu, 75005 Paris, France*

[b] *Matière et Systèmes Complexes, FR2438, France*

[c] *Laboratoire des Liquides Ioniques et Interfaces Chargées, Université Pierre et Marie Curie, Bâtiment F, Case 63, 4 place Jussieu, 75005 Paris, France*

Received 22 May 2002; accepted 9 September 2002

Abstract

A new class of superparamagnetic nanoparticles bearing negative surface charges is presented. These anionic nanoparticles show a high affinity for the cell membrane and, as a consequence, are captured by cells with an efficiency three orders of magnitude higher than the widely used dextran-coated iron oxide nanoparticles. The surface coating of anionic particle with albumin strongly reduces the non specific interactions with the plasma membrane as well as the overall cell uptake and at the same time restores the ability to induce specific interactions with targeted cells by the coadsorption on the particle surface of a specific ligand. Kinetics of cellular particle uptake for different cell lines are quantitated using two new complementary assays (Magnetophoresis and Electron Spin Resonance).

Keywords: Superparamagnetic nanoparticles; Endocytosis; Cellular uptake; Surface coating

1. Introduction

Cell labeling with magnetic nanoparticles is an increasingly common method for in vitro cell separation as well as for in vivo imaging owing to their signal amplification properties in magnetic resonance imaging (MRI). Magnetic cell labeling also raises very promising developments for therapy, by allowing magnetic intracellular hyperthermia [1,2]. All these applications require that cells efficiently capture the magnetic nanoparticles either in vitro or in vivo. In vivo, requisites for cell targeting are to graft high affinity ligands on the nanoparticles surface in order to favor specific interactions [3] and, at the same time, to prevent the interactions with serum protein and subsequent capture by the reticuloendothelial system. In vitro, magnetic labeling only needs a high capture of the nanoparticles by the cells, following the endocytosis pathway. Beyond interesting developments in cell biology (to purify or to manipulate magnetically intracellular organelles) [4,5], an efficient in vitro magnetic labeling offers promising new approaches in cell-based therapy. The cells of interest (for instance T lymphocytes [6] or stem cells [7]) are isolated and labeled in vitro before their transplantation in vivo [8–10]. It is then possible to track their migration in vivo (homing or recruitment for example) by high resolution MRI [7] thanks to the signal amplification due to the magnetic properties of the labeled cells. The most commonly used iron oxide nanoparticles are dextran coated [11] but do not present sufficient cellular uptake to enable cell tracking, probably because of a relatively inefficient fluid phase endocytosis pathway. However, significant improvements in the magnetic labeling efficiency and versatility were achieved by the attachment on the nanoparticles surface of a transfection agent or a small peptide, known to facilitate cell internalization [7,12].

In this paper, we present a new class of iron oxide nanoparticles, anionic maghemite nanoparticles (AMNP). We demonstrate that it is a highly versatile system suitable either for a high efficiency non specific cellular uptake mediated by adsorptive endocytosis

*Corresponding author. Universitè Pierre et Marie Curie, UMR7603, Tour 13, Case 86, 4 place Jussieu, Paris 75005, France.
E-mail address: floga@ccr.jussieu.fr (F. Gazeau).

0142-9612/02/$ - see front matter © 2002 Elsevier Science Ltd. All rights reserved.
PII: S0142-9612(02)00440-4

(using bare AMNP), either for specific cell recognition allowed by the nanoparticle surface modification and the binding of a specific ligand. We show that bare anionic maghemite nanoparticles, free of any dextran coating, exhibit a surprisingly high level of cell internalization that is comparable with nanoparticles modified with Tat peptide [12] or encapsulated into dendrimers [7]. They interact strongly and non specifically with the plasma membrane thanks to their surface negative charges. This adsorption step, which appears to be ubiquitous, precedes the internalization step and governs the overall cell uptake. Alternatively, to induce receptor mediated endocytosis pathway and cell specific magnetic labeling, it is necessary to reduce the non specific nanoparticles/membrane interactions and to force the recognition of the nanoparticles by the membrane receptors. We show that the non specific adsorptive endocytosis pathway can be inhibited by steric hindrance, due to the coating of the AMNP surface with albumin or with dextran. We also demonstrate that AMNP coated with albumin are good candidates for the binding on the nanoparticle surface of a cell membrane high affinity ligand, like an antibody.

In the present paper, the surface modifications and the colloidal stability of the anionic maghemite nanoparticles are characterized by a new method, magnetically induced birefringence measurement, that is sensitive to the hydrodynamic volume of the particles. Cell uptake assays are performed for comparison with AMNP, with BSA-coated AMNP and with dextran coated iron oxide nanoparticles. Quantification of particle uptake is obtained using new complementary magnetic assays, magnetophoresis (MP) and electron spin resonance (ESR).

2. Materials and methods

2.1. Synthesis and characterization of anionic maghemite nanoparticles (AMNP)

2.1.1. Chemical synthesis

The iron oxide nanoparticles studied in this work are made of maghemite (γFe_2O_3), a ferrimagnetic crystal with an inverse spinel structure: $\left[Fe^{III}\right]_A\left[Fe^{III}_{5/3}\Delta_{1/3}\right]_B O_4$ where A and B stand, respectively, for tetraedric and octaedric sites, and Δ stands for lacuna. The ionic precursor is synthesized according to the Massart's method [13] by alkalizing an aqueous mixture of iron (II) chloride and iron (III) chloride. With use of $Fe(NO_3)_3$, the so obtained magnetite (Fe_3O_4 : $\left[Fe^{III}\right]_A\left[Fe^{III}Fe^{II}\right]_B O_4$) nanoparticles are then oxidized into the more stable maghemite (γFe_2O_3) and dispersed into water. According to the process described elsewhere [14,15], nanoparticles are then chelated with *meso-2,3-dimercaptosuccinic acid* (HOOC-CH(SH))-CH(SH)-COOH) or DMSA, which forms strong complexes with the surface layer of the nanoparticle. One finally obtains an aqueous sol of thiolated maghemite nanoparticles, which is stable in a large pH range (from 3 to 11), in suitable ionic strength (<0.35 mol/l) and in various buffers such as Hepes. In the current report, the AMNP are dispersed in Hepes 0.1 M at pH 7.4. The surface charges are mainly due to unbound carboxylate groups (COO^-) and electrostatic repulsions between the charged nanoparticles ensure the colloidal stability [16]. Note that there exist SH groups remaining free on the nanoparticle surface which can be used to covalently graft a biological effector to the nanoparticle via S-S bridge or S-C bridge [15]. However, in this paper, we study either "bare" nanoparticles bearing only DMSA ligands, either DMSA-nanoparticles with a surface modified by the physisorption of albumin and immunoglobulin.

2.1.2. Magnetic properties

Transmission electron microscopy (TEM) show that the nanoparticles are roughly spherical and polydisperse ($3\,nm < D_{TEM} < 15\,nm$). They consist of monocrystalline ferrimagnetic monodomain of maghemite. The magnetic core diameter distribution is obtained from analyzing the magnetization curve of the aqueous suspension of the nanoparticles as described earlier [17]. For the nanoparticles used in this study, this distribution is well described by a lognormal distribution with a mean magnetic diameter $d_{mag} = 8.7\,nm$ (corresponding to 13700 iron atoms per nanoparticle) and standard deviation $\sigma = 0.357$. The saturation magnetization of each nanoparticle is $M_s = 3.1 \times 10^5\,A\,m^{-1}$ per unit volume. The properties of AMNP as contrast agent in MRI are described elsewhere [18]: we find at 25°C and at 1.5 T (clinical MRI) for AMNP in water the longitudinal relaxivity $R_1 = 11.6\,s^{-1}\,mM^{-1}$ and transverse relaxivity $R_2 = 363.2\,s^{-1}\,mM^{-1}$ with a ratio $R_2/R_1 = 31.3$.

2.2. Surface modification of anionic maghemite nanoparticles

2.2.1. Coating with bovine serum albumin

In order to coat the AMNP surface with albumin, bovine serum albumin (BSA) (molecular mass 66.4 kDa and isoelectric point about 5) is incubated at 4°C overnight with an aqueous suspension of AMNP ([Fe] = 0.2 M), at various concentrations: 0–5% in mass, corresponding to an initial molar ratio [BSA]/[AMNP] varying from 0 to 50. The nanoparticles suspension is then purified two times by ultrafiltration in a 100 kDa Macrosep filter (Filtron) centrifugated at 3000 rpm during 45 min.

2.2.2. IgG adsorption on AMNP previously coated with Bovine Serum Albumin

For the nanoparticles/ IgG binding assay, the antibody is a polyclonal purified bovine IgG (Immunoglobulin G, Sigma, ref15506) isolated from pooled normal bovine serum. Different quantities of purified bovine IgG (molecular weight 150 kDa) are added to 1.5 ml of a suspension of BSA coated particles (initial molar ratio [BSA]/[AMNP] = 5), both in Hepes 0.1 M, at pH = 7.5 and with an iron concentration [Fe] = 0.2 M (measured by atomic absorption). The inital molar ratio [IgG]/[BSA – coated AMNP] varies from 0 to 0.96. The mixture is then incubated overnight at 4°C and purified by ultrafiltration as described above.

2.3. Dextran-coated nanoparticles

To evaluate the role of surface coating on the cell uptake efficiency, cell uptake assays are simultaneously performed with AMNP and dextran-coated magnetic nanoparticles (Ferumoxtran developed by Advanced Magnetics Inc., Cambridge, MA. and also known as USPIO, AMI-227, BMS 180549; trade name Sinerem in Europe (laboratoire Guerbet)) which are widely used as contrast agents in MRI, undergoing clinical developments. Physical properties of these dextran coated iron oxide nanoparticles are described in detail in [19–21]. They consist of nonstoechiometric magnetite monocrystalline and monodomain cores with mean diameter 5 nm (comprising about 2600 iron atoms) presenting analogous superparamagnetic properties as AMNP. The magnetic cores are coated with dextran T-10 (22 nm average chain length) and thus stabilized in suspension by steric repulsions.

2.4. Characterization of surface modification: measure of nanoparticle hydrodynamic diameter by magnetically induced optical birefringence assay

The hydrodynamic volume of the nanoparticles surrounded by their eventual coat, is probed through a magnetically induced birefringence experiment which is described elsewhere in details [22]. The optical birefringence induced by an external magnetic field in a suspension of magnetic nanoparticles results from the combined effect of the alignment of nanoparticle magnetic moments along the field and the subsequent alignment of their optical anisotropy axes [23]. The relaxation in zero field of the birefringence follows a stretched exponential law, $I(t)/I_0 = \exp(-(t/\tau)^{\alpha})$, reflecting the distribution of orientational Brownian relaxation times of the nanoparticles in suspension. The characteristic time for a nanoparticle to loose its orientation due to thermal orientational fluctuations writes

$$\tau = \frac{\eta}{k_B T}\pi/6\, d_{hyd}^3,$$

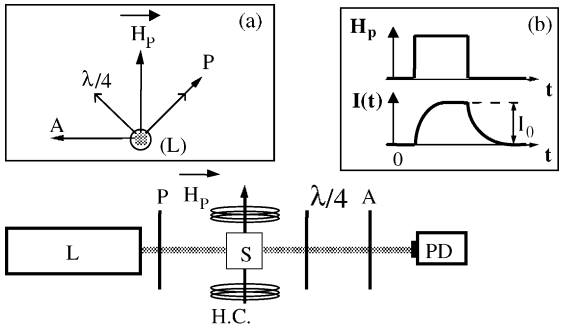

Fig. 1. Experimental setup for the birefringence measurements. Part (a) presents the orientations of the different optical axes. *A*: analyser, *P*: polarizer, *L*:He-Ne laser, HC: Helmholtz Coils, *PD*: Photodetector, *S*: sample. Part (b) shows the pulse of the magnetic field H_P and the corresponding time dependence of transmitted light intensity $I(t)$. I_0 is the saturation value of the light intensity under the magnetic field H_P.

where η is the viscosity of the carrier fluid, T the temperature, k_B the Boltzmann constant and d_{hyd} the hydrodynamic diameter of the nanoparticle in suspension. From the analysis of the birefringence relaxation, we deduce the distribution of hydrodynamic diameter d_{hyd}, characterized by a characteristic diameter d_0 and a polydispersity index α (the smaller $\alpha \leqslant 1$, the larger the distribution; $\alpha = 1$ corresponding to a monodisperse suspension) [22]. The sketch of the optical set up is represented in Fig. 1. The suspension of nanoparticles is put in a non birefringent glass chamber (thickness $e = 200\,\mu m$) and probed by a He-Ne laser beam (L) of weak power (≈ 5 mW) and wavelength $\lambda_0 = 632.8$ nm. The suspension behaves as a birefringent plate characterized by a phase lag φ related to its birefringence Δn. Δn is defined as $\Delta n = n_{\parallel} - n_{\perp}$, $n_{\parallel}$ being the optical index in the direction of the magnetic field and $n_{\perp}$ the optical index in the perpendicular direction. For a sample of thickness e, the phase lag is $\varphi = 2\pi e \Delta n/\lambda_0$. The polarization of the transmitted light measured by a photodetector (PD) is analyzed using a polarizer (P), a quaterwave plate ($\lambda/4$), an analyzer (A) with respective directions indicated in the part a of Fig. 1. The nanoparticles suspension is submitted to a pulsed vertical magnetic field ($H_p = 12$ kA/m) produced by Helmholtz's coils (HC). When the magnetic field is switched on, the light intensity $I(t)$ (proportional to φ in the limit of small phase lag φ) increases towards a saturation value I_0. The field is then switched off and the decrease of transmitted light is measured (see part b of Fig. 1).

2.5. Cell models and magnetic labeling

Experiments are made on a culture line of mouse macrophages (RAW 264.7) and human ovarian tumor cells (HeLa). Cells are grown in DMEM medium supplemented with 10% heat inactivated fetal calf

serum, 50 U/ml penicillin, 40 mg/ml streptomycin and 0.3 mg/ml L-glutamine. Cells diameter measured on spherical cells in suspension is higher for HeLa cells ($20.2 \pm 0.8\,\mu m$) than for RAW macrophages ($11.7 \pm 0.5\,\mu m$). Cell labeling is performed by adding filter-sterilized suspension of magnetic nanoparticles in serum free culture medium (5 ml, 10^6 cells). Cells are incubated either at 37°C, either at 4°C for different incubation times (15 min to 12 h) and various extracellular iron concentrations (0.1 mM–20 mM).

2.6. Transmission electron microscopy (TEM)

After magnetic labeling and chase, adhering cells are washed 2 times with 0.1 M cacodylate buffer and then incubated in 2% glutaraldehyde in cacodylate buffer for 1 h at 4°C. Cells are then postfixed in 1% OsO_4 for 2 h at 4°C, washed again with cacodylate buffer, dehydrated in an alcohol series and embedded in Epon. Ultrathin sections of 70 nm are examined with a JEOL120CX transmission electron microscope.

2.7. Quantification of magnetic particle cellular uptake

Two different assays, magnetophoresis and ESR, described in detail in [24] have been designed to measure the cellular magnetic particle uptake.

2.7.1. Magnetophoresis (MP)

The magnetophoresis assay consists in measuring the velocity of magnetically labeled cells in suspension when they are submitted to a magnetic field gradient. After being scrapped, cells are introduced into a 1mm thick Hellma chamber previously treated with dimethyldichlorosilane to prevent the cells from adhering on the glass. An inverted microscope was adapted to accommodate a permanent magnet which creates a horizontal magnetic field ($\vec{B} = B\vec{e}_z, B = 174$ mT in the observation window) and a uniform magnetic field gradient ($\vec{\nabla}B = \mathrm{d}B/\mathrm{d}z\vec{e}_z, \mathrm{d}B/\mathrm{d}z = 18.5$ mT/mm). The sketch of the experiment is given in Fig. 2a. The horizontal z component of cell velocity, v, due to the field gradient (perpendicular to the optical axis and to the gravity) is measured from video analysis. In permanent regime, v is governed by the balance between the magnetic force $F_{mag} = N\mu\,\mathrm{d}B/\mathrm{d}z$ and the viscous force $F_{visq} = -6\pi\eta Rv$ where N is the number of internalized nanoparticles, μ the particle magnetization in the field B (thus $N\mu$ is the magnetic moment of the cell), η the viscosity of the carrier fluid and R the cell radius (here cells in suspension are assimilated to spheres). N is thus given for each cell by

$$N = \frac{6\pi\eta Rv}{\mu(\mathrm{d}B/\mathrm{d}z)},$$

with $\eta = 10^{-3}$ Poiseuille, $\mu \simeq 0.75 \times M_s V$ ($V = \frac{\pi}{6}d_{mag}^3$ is the mean particle volume). We measure the velocity v and the radius R of a hundred cells migrating towards the magnet. For each incubation condition we obtain the distribution of the number N of nanoparticles per cell, or equivalently the iron mass $m(\mathrm{pg}) = 1.23 \times 10^{-6}$ N loaded by cell, as illustrated in Fig. 2b. We deduce the mean iron load as reported in quantitation curves and its statistical deviation for one cell population reflecting the variability of uptake ability from cell to cell.

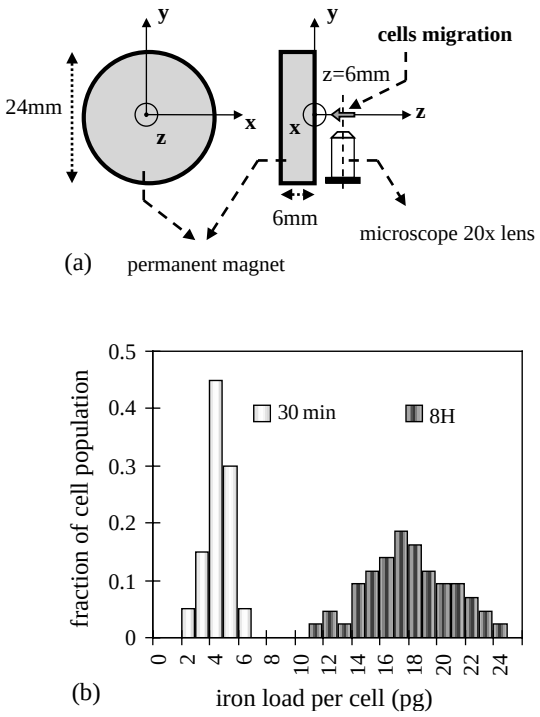

Fig. 2. (a) Sketch of the magnetophoresis setup. The Hellma chamber containing magnetically labeled cells in suspension is placed perpendicularly to the circular permanent magnet. The magnet is placed at 6 mm of the center of the microscope lens so that cell migration is video recorded in a fixed observation window. (b) Typical distributions of the iron mass loaded per cell deduced from the velocity measurements of 100 magnetically labeled HeLa cells (30 min and 8 h incubation, [Fe] = 1.5 mM).

2.7.2. Electron spin resonance

Electron spin resonance (ESR) is a very sensitive method to study or detect species with unpaired electron, in particular superparamagnetic nanoparticles [25]. The ESR signal is obtained by sweeping the static field H and recording the microwave absorption for an excitation field at 9.2 GHz. The measured signal is the derivative of the absorbed power $\partial P/\partial H$ with respect to the constant magnetic field H and as a function of H. The integral $\int P(H)\,\mathrm{d}H$ is a linear function of the amount of maghemite nanoparticles present in the sample (calibration made with aqueous colloidal suspensions of the different particles used in this study, for iron concentrations varying from 0.05 to 50 mM in a 2 μl

volume). Amounts as low as 10^{-10} mole of iron, corresponding to 4.5×10^9 maghemite particles can be measured in a sample volume as tiny as a few μl. Cell sample preparation is the following: after magnetic labeling, the adherent cells are washed 3 times with culture medium, scrapped and centrifugated at 1100 rpm for 10 min. The supernatant is aspirated carefully and 2 μl of the pellet (containing a known number of cells, about 3×10^5) is introduced in a glass capillar, which is placed in a quartz tube suitable for ESR experiment. The iron content of the cell sample is then measured and the iron load by cell is deduced from the number of cells in the sample.

3. Results

3.1. Particle surface modification

We have shown in a previous paper [22] that the measurement of the magnetically induced birefringence relaxation, providing the distribution of hydrodynamic diameters of superparamagnetic nanoparticles, allowed to detect the binding reaction of a macromolecule on the nanoparticle surface and moreover the eventual onset of nanoparticle aggregation. The robustness of the method was proved by comparing nanoparticles fractionated in size by gel filtration. In the present paper, we use this method to characterize quantitatively the adsorption of albumin on anionic magnetic nanoparticles in order to point out its influence on the cell uptake. To show the versatility of the anionic maghemite nanoparticles, we also mention above our previous finding (detailed in [22]) that anionic nanoparticles coated with albumin can efficiently adsorb polyclonal antibodies without affecting the colloidal stability of the suspension.

3.1.1. BSA adsorption on AMNP

Bare AMNP are characterized using the magnetically induced birefringence assay by a characteristic hydrodynamic diameter $d_0 = 34.7 \pm 0.5$ nm and a polydispersity index $\alpha = 0.86$, with a diameter distribution represented in Fig. 3b. The birefringence assay allows to demonstrate the efficient adsorption of BSA on the AMNP surface, after incubation at 4°C overnight : the characteristic hydrodynamic diameter d_0 of the nanoparticles grows from 35 to 46 nm as the initial ratio [BSA]/[AMNP] is varied from 0 to 50 (see Fig. 3a). The polydispersity index does not vary notably except for the low values of [BSA]/[AMNP]. The whole diameter distribution (represented in Fig. 3b for [BSA]/[AMNP] = 5) is shifted compared to the diameter distribution of bare particles. In the range of low initial ratios ([BSA]/[AMNP] < 10), the hydrodynamic diameter rapidly increases together with the polydispersity

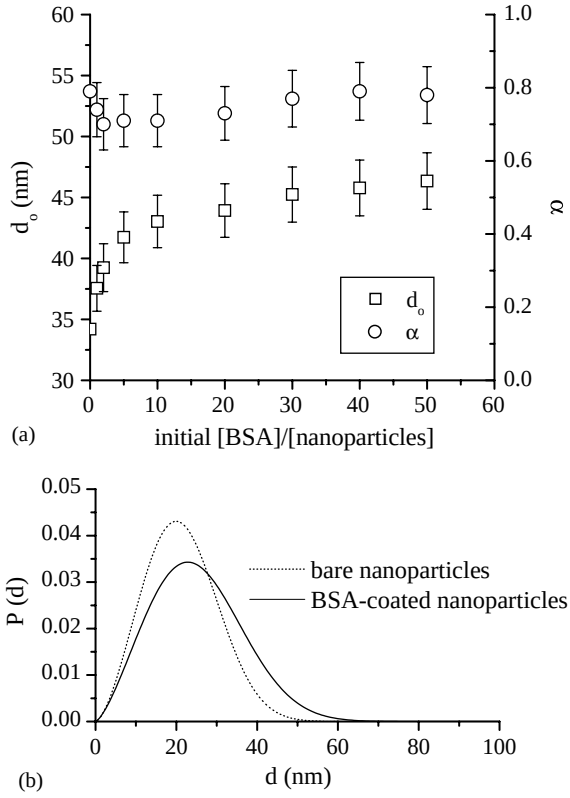

Fig. 3. (a) Hydrodynamic diameter d_0 and polydispersity index α deduced from birefringence experiments on BSA-coated AMNP. Particles are incubated with an initial [BSA]/[AMNP] ratio varying from 0 to 50, inducing an increase of d_0 of about 10 nm which reflects the effective adsorption of BSA on the nanoparticle surface. (b) Comparison of the hydrodynamic diameter distribution for bare AMNP and for BSA-coated AMNP (initial ratio [BSA]/[AMNP] = 5).

(α is lowered), likely because an increasing proportion of nanoparticles bearing one *BSA* coexists with bare nanoparticles. For higher ratio, the proportion of bare nanoparticles tends to zero, resulting in a sharper distribution of hydrodynamic diameters and a saturation of d_0. Hydrodynamic diameters d_o and polydispersity index α have been measured for nanoparticles with initial ratio [BSA]/[AMNP] = 20, up to 30 days after the preparation: no variation is observed, demonstrating both the stability of the albumin coating and the absence of time dependent nanoparticle aggregation.

3.1.2. IgG adsorption on BSA-coated AMNP

Birefringence relaxations were measured for suspension of BSA-coated AMNP incubated with *IgG* (4°C, overnight) at initial ratio [IgG]/[BSA − coated AMNP] varying from 0 to 0.96. Fig. 4 illustrates the characteristic hydrodynamic diameter d_o of nanoparticles as a function of the ratio [IgG]/[BSA − coated AMNP]. Increasing R, d_0 increases linearly, showing that the

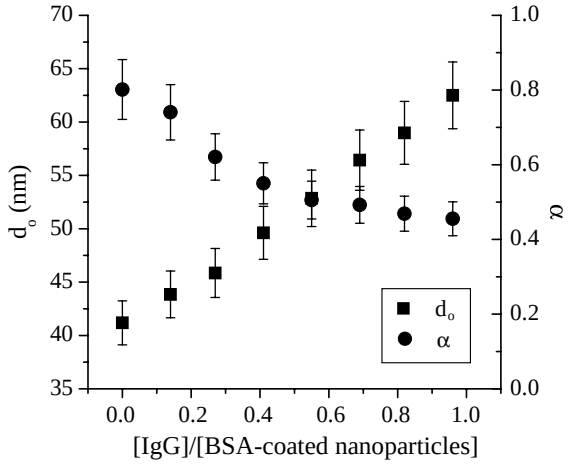

Fig. 4. IgG binding assay on BSA-coated nanoparticles: characteristic hydrodynamic diameter d_0 and polydispersity index α as a function of the ratio [IgG]/[BSA-coated AMNP].

antibody is adsorbed on the nanoparticle surface without inducing particles aggregation or antibodies cross-linking. We hypothesize that the negatively charged BSA proteins previously adsorbed on the nanoparticles surface strengthen the electrostatic repulsions between nanoparticles and simultaneously create steric repulsions which are unfair to multiple antibody linking. Thus, from the point of view of colloidal stability, AMNP coated with BSA are suitable for the coupling of specific ligands in order to trigger specific recognition by cell receptors.

3.2. Cellular uptake

3.2.1. Internalization pathway of anionic maghemite nanoparticles

TEM was performed on different cell lines and at different stages of the capture process of AMNP. Fig. 5a shows a TEM picture of a HeLa cell fixed after 1h incubation at 4°C (endocytosis inhibited) with bare AMNP ([Fe] = 20 mM) and illustrates the adhesion of the anionic nanoparticles on the plasma membrane mainly on the form of clusters and probably via electrostatic interactions. Figs. 5b and c correspond to the same incubation (1 h at 4°C, [Fe] = 20 mM) but followed by chase at 37°C, restoring the endocytosis activity. Early events of cell internalization, in particular clathrin coated vesicles containing nanoparticles, are visible in Fig. 5b (10 min chase) and densely confined AMNP into endocytic organelles with various morphological features and cytoplasmic localizations (late endosomes and lysosomes with micrometric size) are observed in Fig. 5c (1 h chase). Similar endosomal labeling is obtained for mouse macrophages RAW.

3.2.2. Cellular uptake of anionic maghemite nanoparticles (AMNP)

The particle uptake in HeLa cells and RAW macrophages is quantified comparatively with the magnetophoresis method (MP) and the ESR method, showing for all quantitation curves a remarkable agreement, though these methods are based on different physical concepts. On one hand, to investigate the nanoparticles binding to the plasma membrane independently of their internalization within the cell, magnetic labeling is performed at 4°C (endocytosis inhibited). The mass of nanoparticles bound on HeLa and RAW cell surfaces as a function of the extracellular iron concentrations after 1 h incubation time at 4°C is represented in Fig. 6a, both curves presenting saturable binding. On the other hand, Figs. 6b and c show the evolution of the mass of iron $m(t)$ loaded per cell as a function of the incubation time at 37°C, respectively, for HeLa cells (iron concentration in the extracellular medium [Fe] = 1.5 and 15 mM) and for RAW macrophages ([Fe] = 0.75 and 1.5 mM). Both cell lines present saturable uptake. Note that the mass of anionic particles adsorbed on the cell membrane at 4°C, as well as the total uptake at 37°C is larger for HeLa cells than for RAW macrophages.

3.2.3. Cellular uptake of BSA-coated AMNP

In this section, we investigate the role of albumin surface coating on the nanoparticle/membrane interactions and on the subsequent cellular internalization. For this purpose, in a first step HeLa cells were incubated during 4 h at 4°C (in serum free and BSA free medium) with AMNP ([Fe] = 15 mM) previously incubated with increasing initial ratio [BSA]/[AMNP]. As shown in Fig. 7, the mass of nanoparticles attached to the cell surface decreases exponentially as the ratio [BSA]/[AMNP] is increased.

In a second step, we performed incubations of BSA coated nanoparticles (initial [BSA]/[AMNP] = 20) with HeLa cells and RAW macrophages at 37°C ([Fe] = 15 mM): the uptake of BSA-coated AMNP, represented as a function of incubation time in Fig. 8a, appears to be considerably lower (saturating around 8 pg per macrophage and 3 pg per HeLa cell) compared to uncoated AMNP (about 40 pg per HeLa cell at saturation in the same incubation conditions, (see Fig. 6b)) and more efficient in macrophages than in HeLa cells.

3.2.4. Cellular uptake of dextran-coated nanoparticles

We compare the uptake of AMNP with dextran-coated nanoparticles. Fig. 8b presents the mass of dextran-coated particles loaded per HeLa cell and per RAW macrophage as a function of incubation time for an extracellular iron concentration [Fe] = 15 mM. Dextran-coated particle uptake attains 0.38 pg in RAW

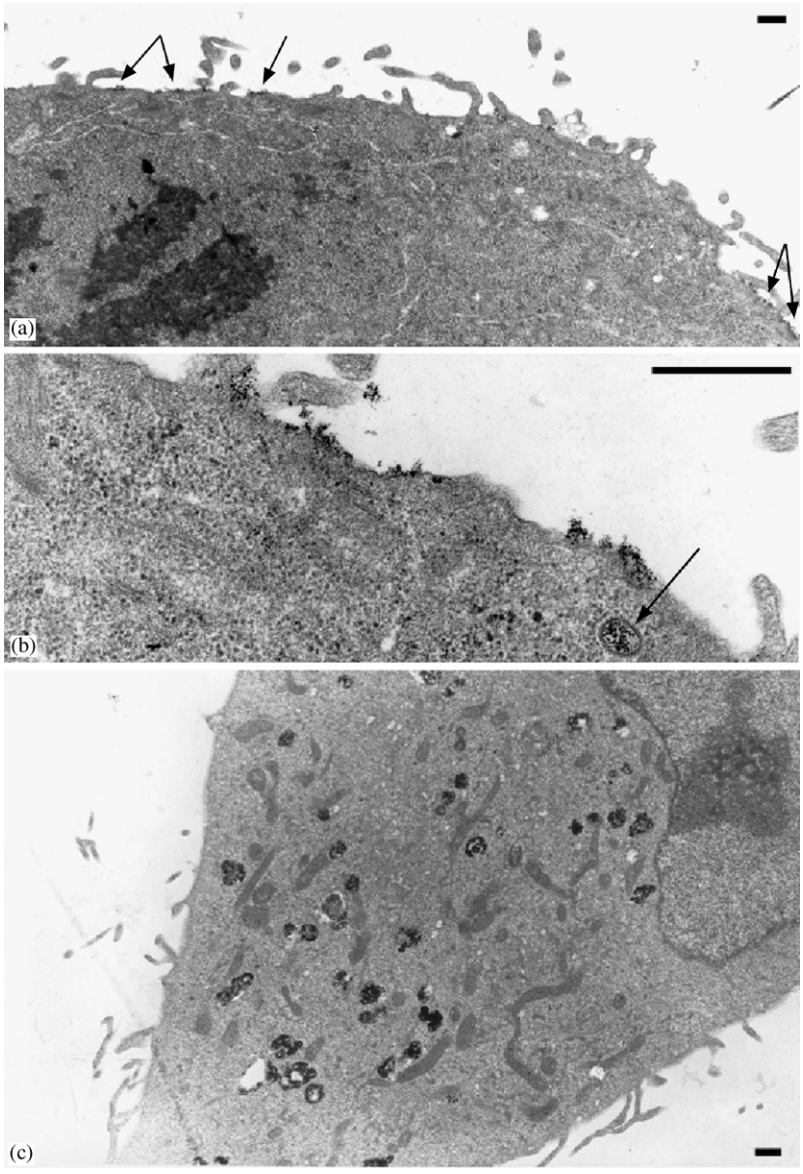

Fig. 5. Transmission electron micrograph of a HeLa cell (a) fixed after 1 h incubation with AMNP at 4°C ([Fe] = 20 mM). One observes the adsorption of nanoparticles on the plasma membrane mainly on the form of clusters (arrows); (b) fixed after 1 h incubation with AMNP at 4°C ([Fe] = 20 mM) and 10min chase at 37°C. Particles are present within invaginations of the cell membrane and within (eventually clathrin coated) early endosomes (arrow); (c) fixed after 1h incubation at 4°C with AMNP ([Fe] = 20 mM) and 1 h chase at 37°C. The anionic nanoparticles are densely confined into numerous late endosomes and lysosomes. Bar stands for 1 μm.

macrophages and 0.05 pg in HeLa cells after 9 H incubation at 37°C.

4. Discussion

4.1. Anionic nanoparticles versus dextran-coated nanoparticles

The capture of anionic nanoparticles by HeLa cells (Fig. 6b) exceeds the capture of dextran-coated iron oxide nanoparticles (Fig. 8b) by three orders of magnitude. For RAW macrophages, the difference is slightly less pronounced, since they capture a smaller amount of anionic particles than HeLa cells, whereas the inverse effect is observed for dextran-coated nanoparticles. Previous studies reported cellular uptake of dextran-coated nanoparticles varying from 0.011 to 0.118 pg of iron per cells (1 h incubation at 37°C, [Fe] = 2 mM) in different tumor cells and a maximum load of 0.97 pg in primary isolated peritoneal mouse macrophages [11,26,27]. By contrast, we evidence saturating uptake of anionic nanoparticles up to 40 pg per cell in HeLa cells for [Fe] = 15 mM (Fig. 6b) and up to 10 pg per cell in macrophages for [Fe] = 1.5 mM (Fig. 6c). An important feature distinguishing both types of nanoparticles is

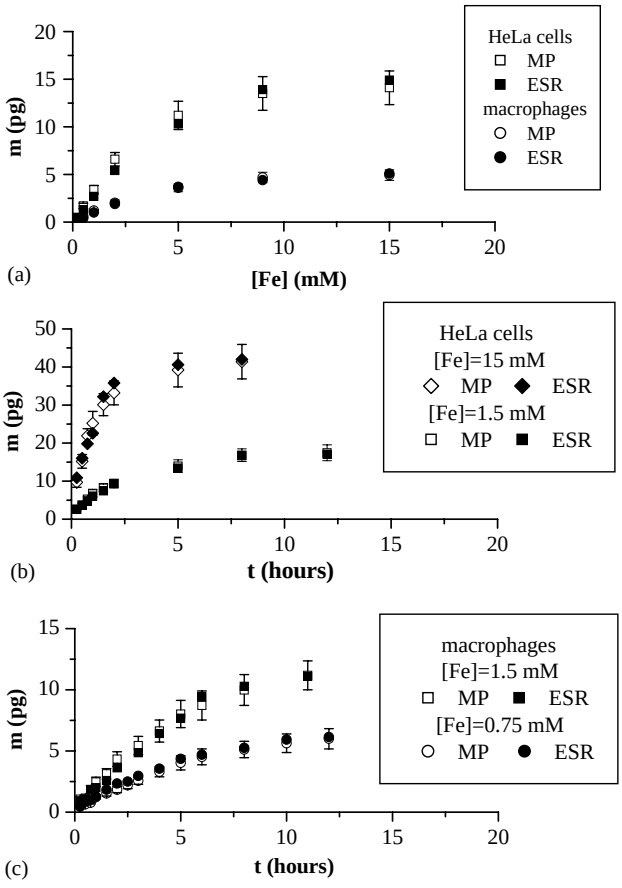

Fig. 6. Magnetophoresis (MP) and Electronic Spin Resonance (ESR) quantitations of AMNP uptake (a) for both HeLa and RAW macrophages at 4°C after 1 h incubation as a function of extracellular iron concentration [Fe]; (b) for HeLa cells at 37°C as a function of incubation time t for two extracellular iron concentrations [Fe] = 1.5 and 15 mM; (c) for RAW macrophages at 37°C as a function of incubation time t for two extracellular iron concentrations [Fe] = 0.75 and 1.5 mM. m (in pg) is the iron load per cell.

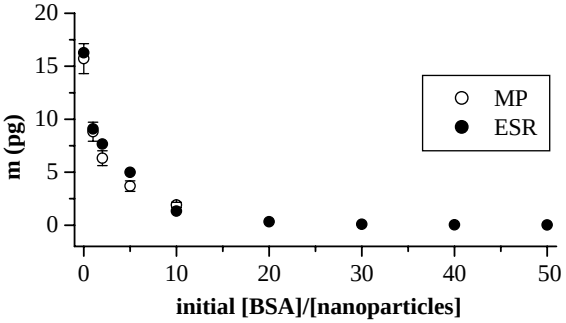

Fig. 7. Magnetophoresis (MP) and Electronic Spin Resonance (ESR) quantitations of BSA-coated AMNP uptake in HeLa cells after 1 h incubation at 4°C as a function of the initial ratio [BSA]/[AMNP] for [Fe] = 15 mM.

that dextran-coated particles show non saturable internalization as claimed in [27] and verified on Fig. 8b, whereas the AMNP uptake saturates both with incubation time and with extracellular concentration at 37°C and at 4°C (Fig. 6). The non saturable internalization of

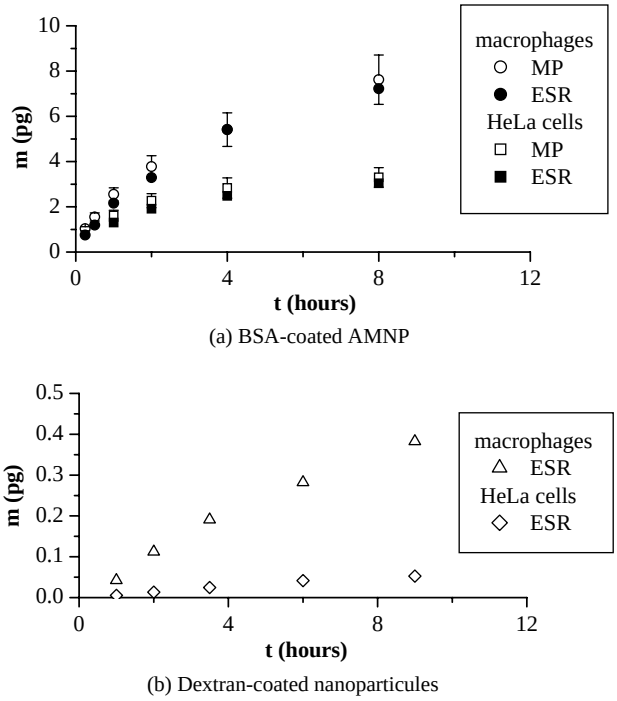

Fig. 8. (a) Magnetophoresis (MP) and Electronic Spin Resonance (ESR) quantitations of BSA-coated AMNP uptake in both HeLa and RAW cells at 37°C as a function of incubation time t for [Fe] = 15 mM and initial ratio [BSA]/[AMNP] = 20. (b) Electronic Spin Resonance (ESR) quantitation of the dextran-coated particles uptake in both HeLa and RAW cells at 37°C as a function of incubation time t for [Fe] = 15 mM. m (in pg) is the iron load per cell.

dextran nanoparticles with limited efficiency suggests that fluid phase endocytosis is the mechanism of uptake. Moreover, competition assay with free dextran did not reveal any significant inhibition of endocytosis and there exist no known binding centers for dextran on the plasma membrane [27]. The huge difference in cell uptake efficacy between anionic and dextran-coated nanoparticles is thus probably related to the lack of efficient binding of dextran nanoparticles on the plasma membrane, which limits the capability of cell internalization to the fluid phase endocytosis pathway.

4.2. Adsorptive endocytosis of AMNP: role of electrostatic interaction

In order to understand the unsuspected high level of internalization of anionic nanoparticles both in macrophages and in tumor cells, we emphasize that the cell uptake can be viewed as a two-step process : first a binding step on the cell membrane and second the internalization step. Both steps occur concomitently at 37°C, whereas only the initial binding occurs at 4°C. Uptake assays performed at 4°C show that anionic nanoparticles adsorb on the cell membrane following dose dependent saturable kinetics (Fig. 6a). Normalized by the cell surface (assuming a binding area of $2\pi R^2$,

where R is the radius of the spherical cell in suspension), the binding capacity per unit surface is $0.028 \pm 0.0023\,\mathrm{pg}/\mu\mathrm{m}^2$ or $2.3\,10^4 \pm 1.9\,10^3\,\mathrm{particles}/\mu\mathrm{m}^2$ and is found identical for both HeLa cells and RAW macrophages. This result allows to conclude that the interactions of anionic particles with the plasma membrane are triggered by saturable reactive sites that we do not identify in this paper and that these reactive sites are involved both in RAW and HeLa cells with the same surface density. Thus it is likely that the adsorption of anionic nanoparticles on the cell membrane does not depend of cell specificity. The particularity of anionic nanoparticles compared to the widely used dextran-coated nanoparticles lies first in their surface negative charges, mainly due to carboxylate groups and second in the absence of any steric coating. The chemical structure of DMSA should not play a decisive role in the nanoparticles/membrane interactions since negatively charged citrate coated nanoparticles present similar high level of cell uptake (results non shown). We thus hypothesize that electrostatic interactions govern the adsorption of the anionic nanoparticles onto the cell membrane. It is known however that plasma membranes possess large negatively charged domains, which should repel anionic nanoparticles. Comparatively, cationic sites are scarcer on the plasma membrane, but are revealed by the possible adsorption of anionic ferritin (with typical size 11 nm) [28,29], smaller charged markers such as anionized hemoundecapeptide [30] and eventually negatively charged liposomes (with typical size 100 nm) [31,32]. As anionized ferritin, anionic maghemite nanoparticles bind on the cell surface on the form of clusters probably because of their repulsive interactions with the large negatively charged domains of the cell surface. In addition, the nanoparticles, already bound on the cell surface present a reduced charge density, that may favor their aggregation with other free nanoparticles. As a conclusion, the high efficiency of anionic nanoparticles cell uptake seems to be related first to the non specific process of nanoparticles adsorption on the cell membrane and second to the formation of nanoparticles clusters. Contrary to the adsorption process, the internalization capacity, as itself, depends of the cell types but should not dominate the overall uptake of these anionic nanoparticles.

4.3. AMNP versus engineered magnetic nanoparticles for high efficiency cellular uptake

In the last years, different strategies have been employed in an effort to improve the efficiency of magnetic labeling of a wide variety of cells. First strategy is to substitute to the fluid phase endocytosis pathway the more efficient receptor mediated endocytosis pathway by coupling dextran-coated particles with specific ligands. Some authors exploited the ubiquitous transferrin receptor to shuttle transferrin-coupled dextran coated nanoparticles into gliosarcoma cells [33,34] as well as into neural progenitors cells [9]. The cell capture of transferrin-coupled nanoparticles was two to four times higher compared to the dextran-coated particles and was dependent upon the level of cell expression of the transferrin receptors. These studies demonstrated the possibility of imaging a gene expression in vivo using targeted superparamagnetic nanoparticles [34]. However, the uptake efficiency remained limited by the number of cell membrane receptors. Another strategy was to combine superparamagnetic nanoparticles with a transmembrane permeabilization agent, known to facilitate the translocation of a wide variety of macromolecules into cells. Some authors [12,10] performed the graft, on a crosslinked dextran-coated superparamagnetic nanoparticles, of a membrane translocating signal peptide, (namely the HIV-1 Tat protein, known to freely travel through cellular and nucleic membranes) and succeeded in improving the magnetic labeling efficiency. Compared to dextran-coated nanoparticles, the uptake was enhanced by two to three orders of magnitude in hematopoietic CD34+ cells, mouse neural progenitor cells, human CD4+ lymphocytes or mouse splenocytes, attaining 10 to 30 pg of iron per cell [12,35]. Besides, the synthesis of superparamagnetic iron oxides encapsulated into dendrimers, known to be a very efficient transfection agent, has allowed to tag HeLa cells as well as CG4 oligodendrocyte progenitors with up to 14 pg of iron per cell [7]. In the two last approaches, the idea was to design magnetic probes to achieve a high degree of intracellular labeling that is *non specific* (and thus virtually applicable to any mammalian cell) because it lies on the high affinity for cellular membrane of an organic shell (dendrimers) or of a virus derived peptide. We demonstrate that comparable labeling efficiency in various cell types can be attained using a system as simple as anionic maghemite nanoparticles. For HeLa cells, as an example, we find an iron load of 17 pg per cell after 12 h incubation with anionic nanoparticles ($[\mathrm{Fe}] = 1.5$ mM) to be compared with an iron load of 13 pg, obtained by [7] using dendrimers encapsulated nanoparticles (48 h incubation with $[\mathrm{Fe}] = 0.5$ mM). For various other cell lines, we measured [24] uptakes of anionic nanoparticles of the same order of magnitude depending essentially of the cell size: human dendritic cells (2.33 pg, incubation 1 h, $[\mathrm{Fe}] = 0.6$ mM), human T-lymphocyte (0.59 pg, incubation 1 h, $[\mathrm{Fe}] = 0.6$ mM), human epithelium A549 cells (4.18 pg, incubation 3 h, $[\mathrm{Fe}] = 0.5$ mM). These comparable degrees of uptake suggest that anionic nanoparticles may serve to label a wide variety of cells. Further uptake assays are in progress to determine the efficiency of AMNP uptake in non dividing and differentiated cells, as well as in

progenitor and stem cells. The analogy of our anionic particles with dendrimers encapsulated particles, allowing comparable labeling efficiency, may lie in their ability to adsorb on the cell membrane through electrostatic interactions. Such as our anionic particles, dendrimers used in [7] possess external carboxylate groups, confering negative surface charges to the magnetic label. Actually, the authors emphasize the role of electrostatic interactions for the nanoparticle adsorption, inducing a local neutralization of the membrane and a subsequent bending of the membrane favoring in turn the formation of endocytosis invaginations. This mechanism has been put forward in the case of high generation polycationic dendrimers that were able to induce the disruption of anionic vesicles [36]. The point which entails new investigations, is to understand if the electrostatic bound between cationic sites on the cell membrane and anionic nanoparticles may favor their internalization through a physical mechanism. In addition, owing to the low density of cationic sites on the cell membrane that are able to attract anionic nanoparticles, the surprisingly high level of cell uptake which is achieved using anionic nanoparticles remains an open question.

4.4. Role of albumin coating on AMNP surface

Birefringence measurements show that the incubation of AMNP with bovine serum albumin results in an efficient adsorption of albumin on the nanoparticles surface (Fig. 3a). As shown in Fig. 7, the consequence of albumin coating is a drastic diminution of their cellular uptake. Note that the initial fall in Fig. 7 coincides with the initial rapid increase of hydrodynamic diameter of BSA-coated nanoparticles (see Fig. 3a), that was interpreted as the result of an increasing proportion of nanoparticles bearing one BSA and coexisting with bare nanoparticles. Thus the overall binding of nanoparticles on the cell is probably dominated by the interactions between the plasma membrane and the bare nanoparticles that are still present in the suspension. By contrast, once the nanoparticles all bear at least one BSA (initial $[BSA]/[AMNP] \geqslant 10$), their fixation to the membrane diminishes drastically and the nanoparticles load becomes hardly detectable even by ESR method. Particle uptake is lowered by two orders of magnitude compared to the bare AMNP for the saturation value of hydrodynamic diameter ($[BSA]/[AMNP] = 50$) (see Fig. 7). Contrary to bare anionic nanoparticles, BSA-coated AMNP are captured more efficiently in macrophages than in Hela cells (see Fig. 8a). This suggests that BSA-coated AMNP and bare AMNP do not interact with the cell membrane in the same way: albumin coating on AMNP hampers their interactions with the plasma membrane probably because of steric effect, which on one part reduces the accessibility of nanoparticles for the positively charged binding sites on the cell membrane and on the other part diminishes the aggregation of the nanoparticles one to the other. Thus the non specific adsorption of nanoparticles on cell membrane is considerably reduced by albumin coating and, as a consequence, cell internalization turns to be limited to the fluid phase endocytosis pathway which may be more efficient in macrophages than in HeLa cells. In some attempts towards specific targeting of anionic maghemite nanoparticles, the coating with albumin appears as a preliminary crucial step to limit the non specific adsorption of the nanoparticles on the cell membrane. In addition, we have shown through birefringence measurements that an immunoglobulin can be bound to the BSA-coated AMNP and that the colloidal stability of the suspension is not affected (Fig. 4). From this point of view, AMNP coated with BSA appears as a suitable system for the coupling of specific ligands in order to trigger specific recognition by cell receptors. Further investigations are necessary to evaluate the targeting ability of these IgG bound BSA-coated AMNP for specific receptors.

5. Conclusion

In summary, anionic maghemite nanoparticles represent a new type of superparamagnetic label that shows a high affinity for cellular membrane mainly due to electrostatic interactions. Their non specific adsorption on virtually any mammalian cells and their subsequent internalization into endosomes offer the opportunity to label a wide variety of cells with comparable efficiency than other magnetic nanoparticles specially engineered to facilitate their entry into cell. It opens up new opportunities for magnetic cell separation and recovery, as well as MR tracking of cell transplant that are of crucial interest for the development of cellular therapies. The non specific interactions with cell membrane, desirable for in vitro cell labeling, can also be inhibited by an albumin coating for different applications requiring either a specific (in vitro or in vivo) targeting or an enhanced in vivo blood circulation.

Acknowledgements

We are grateful to B.de Crossa for preparing electron microscopy samples and to O. Clément and P.-Y. Brillet for their enlightening discussions and for providing dextran coated nanoparticles. This work was financially supported by the CNRS program Physique et Chimie du vivant and by the French research ministry (ACI "Technologies pour la santé").

References

[1] Shinkai M, Le B, Honda H, Yoshikawa K, Shimizu K, Saga S, Wakabayashi T, Yoshida J, Kobayashi T. Targeting hyperthermia for renal cell carcinoma using human MN antigen-specific magnetoliposomes. Jpn J Cancer Res 2001;92(10):1138–45.

[2] Ito A, Shinkai M, Honda H, Kobayashi T. Heat-inducible TNF-alpha gene therapy combined with hyperthermia using magnetic nanoparticles as a novel tumor-targeted therapy. Cancer Gene Ther 2001;8(9):649–54.

[3] Zhang Y, Kohler N, Zhang M. Surface modification of superparamagnetic magnetite nanoparticles and their intracellular uptake. Biomaterials 2002;23:1553–61.

[4] Perrin-Cocon LA, Marche PN, Villiers CL. Purification of intracellular compartments involved in antigen processing: a new method based on magnetic sorting. Biochem J 1999;338: 123–30.

[5] Kausch AP, Owen Jr. TP, Narayanswami S, Bruce BD. Organelle isolation by magnetic immunoabsorption. Biotechniques 1999;26(2):336–43.

[6] Moore A, Zhe Sun P, Cory D, Hogemann D, Weissleder R, Lipes MA. MRI of insulitis in autoimmune diabetes. Magn Reson Med 2002;47(4):751–8.

[7] Bulte JW, Douglas T, Witwer B, Zhang SC, Strable E, Lewis BK, Zywicke H, Miller B, van Gelderen P, Moskowitz BM, Duncan ID, Frank JA. Magnetodendrimers allow endosomal magnetic labeling and in vivo tracking of stem cells. Nat Biotechnol 2001;19(12):1141–7.

[8] Dodd SJ, Williams M, Suhan JP, Williams DS, Koretsky AP, Ho C. Detection of single mammalian cells by high-resolution magnetic resonance imaging. Biophys J 1999;76(1 Pt 1):103–9.

[9] Bulte JW, Zhang S, van Gelderen P, Herynek V, Jordan EK, Duncan ID, Frank JA. Neurotransplantation of magnetically labeled oligodendrocyte progenitors: magnetic resonance tracking of cell migration and myelination. Proc Natl Acad Sci USA 1999;96(26):15256–61.

[10] Lewin M, Carlesso N, Tung CH, Tang XW, Cory D, Scadden DT, Weissleder R. Tat peptide-derivatized magnetic nanoparticles allow in vivo tracking and recovery of progenitor cells. Nat Biotechnol 2000;18(4):410–4.

[11] Moore A, Marecos E, Bogdanov Jr. A, Weissleder R. Tumoral distribution of long-circulating dextran-coated iron oxide nanoparticles in a rodent model. Radiology 2000;214(2):568–74.

[12] Josephson L, Tung CH, Moore A, Weissleder R. High-efficiency intracellular magnetic labeling with novel superparamagnetic-Tat peptide conjugates. Bioconjug Chem 1999;10(2):186–91.

[13] Massart R. Preparation of aqueous magnetic liquids in alkaline and acidic media. IEEE Trans Magn 1981;17:1247.

[14] Fauconnier N, Pons JN, Roger J, Bee A. Thiolation of maghemite nanoparticles by dimercaptosuccinic acid. J Colloid Interface Sci 1997;194:427–33.

[15] Halbreich A, Sabolovic D, Sestier C, Geldwerth D, Pons JN, Roger J. EP 847528A1, US Patent 6, 150, 181, 2000.

[16] Dubois E, Perzynski R, Boué F, Cabuil V. Liquid-gas transitions in charged colloidal dispersions: small angle neutron scattering coupled with phase diagrams of magnetic fluids. Langmuir 2000;16:5617.

[17] Berkovski B. editor. Magnetic fluids and applications handbook. New York: Begell House Inc. Publ., 1996.

[18] Billotey C, Wilhelm C, Bacri JC, Bittoun J, Gazeau F. Cell internalization of anionic maghemite nanoparticles: quantitative effect on Magnetic Resonance Imaging, Magn Reson Med, submitted.

[19] Jung CW. Surface properties of superparamagnetic iron oxide MR contrast agents: ferumoxides, ferumoxtran, ferumoxsil. Magn Reson Imaging 1995;13(5):675–91.

[20] Jung CW, Jacobs P. Physical and chemical properties of superparamagnetic iron oxide MR contrast agents: ferumoxides, ferumoxtran, ferumoxsil. Magn Reson Imaging 1995;13(5): 661–74.

[21] Shen T, Weissleder R, Papisov M, Bogdanov A, Brady T. Monocrystalline iron oxide nanocompounds (MION): physicochemical properties. Magn Reson Med 1993;29:599–604.

[22] Wilhelm C, Gazeau F, Roger J, Pons JN, Salis MF, Perzynski R, Bacri J-C. Binding of biological effectors on magnetic nanoparticles measured by a magnetically induced transient birefringence experiment. Phys Rev E 2002;65(3–1):031404.

[23] Hasmonay E, Dubois E, Bacri JC, Perzynski R, Raikher YuL, Stepanov VI. Static magneto-optical birefringence of size-sorted γFe_2O_3 nanoparticles. Eur Phys J B 1998;5:859–67.

[24] Wilhelm C, Gazeau F, Bacri J-C. Magnetophoresis and ferromagnetic resonance of magnetically labelled cells. Eur Biophys J 2002;31:118–25.

[25] Gazeau F, Shilov V, Bacri JC, Dubois E, Gendron F, Perzynski R, Raikher Yu L, Stepanov VI. Magnetic Resonance of ferrite nanoparticles: evidence of thermofluctuational effects. J Magn Magn Mat 1999;202:535–46.

[26] Schulze E, Ferrucci JT, Poss K, Lapointe L, Bogdanova A, Weissleder R. Cellular uptake and trafficking of a prototypical magnetic iron oxide label in vitro. Invest Radiol 1995;30:604–10.

[27] Moore A, Weissleder R, Bogdanov A. Uptake of dextran-coated monocrystalline iron oxides in tumor cells and macrophages. J Magn Reson Imaging 1997;7:1140–5.

[28] Farquhar MG. Recovery of surface membrane in anterior pituitary cells. Variations in traffic detected with anionic and cationic ferritin. J Cell Biol 1978;77(3):R35–42.

[29] Mutsaers SE, Papadimitriou JM. Surface charge of macrophages and their interaction with charged particles. J Leukoc Biol 1998;44(1):17–20.

[30] Ghinea N, Simionescu N. Anionized and cationized hemeundecapeptides as probes for cell surface charge and permeability studies: differentiated labeling of endothelial plasmalemmal vesicles. J Cell Biol 1983;100(2):606–12.

[31] Lee KD, Nir S, Papahadjopoulos D. Quantitative analysis of liposome-cell interactions in vitro: rate constants of binding and endocytosis with suspension and adherent J774 cells and human monocytes. Biochemistry 1993;32(3):889–99.

[32] Miller CR, Bondurant B, McLean SD, McGovern KA, O'Brien DF. Liposome-cell interactions in vitro: effect of liposome surface charge on the binding and endocytosis of conventional and sterically stabilized liposomes. Biochemistry 1998;37(37):12875–83.

[33] Hogemann D, Josephson L, Weissleder R, Basilion JP. Improvement of MRI probes to allow efficient detection of gene expression. Bioconjug Chem 2000;11(6):941–6.

[34] Weissleder R, Moore A, Mahmood U, Bhorade R, Benveniste H, Chiocca EA, Basilion JP. In vivo magnetic resonance imaging of transgene expression. Nat Med 2000;6(3):351–5.

[35] Dodd CH, Hsu HC, Chu WJ, Yang P, Zhang HG, Mountz Jr. JD, Zinn K, Forder J, Josephson L, Weissleder R, Mountz JM, Mountz JD. Normal T-cell response and in vivo magnetic resonance imaging of T cells loaded with HIV transactivator-peptide-derived superparamagnetic nanoparticles. J Immunol Methods 2001;256(1–2):89–105.

[36] Zhang ZY, Smith BD. High-generation polycationic dendrimers are unusually effective at disrupting anionic vesicles: membrane bending model. Bioconjug Chem 2000;11(6):805–14.